THE ASTROPHYSICAL JOURNAL, 328:143–160, 1988 May 1

OBSERVATIONS OF MOLECULAR AND ATOMIC CLOUDS IN M31

CHARLES J. LADA[1] AND MICHAEL MARGULIS
Steward Observatory, University of Arizona
AND
YOSHIAKI SOFUE, NAOMASA NAKAI, AND TOSHIHIRO HANDA
Nobeyama Radio Observatory and Department of Astronomy, University of Tokyo
Received 1987 April 23; accepted 1987 October 15

ABSTRACT

We report the first coordinated CO and H I observations of M31 made with identical and sufficiently high angular and spectral resolutions to resolve individual giant molecular clouds (GMCs) in that galaxy. We used the C and D arrays of the VLA and the 45 m millimeter-wave telescope of the Nobeyama Radio Observatory to map the 21 cm spin-flip transition of H I and the $J = 1 \rightarrow 0$ transition of CO, respectively, in an individual star-forming complex which is located in an H I spiral arm segment 7 kpc from the center of M31. An angular resolution of 15″, corresponding to a projected linear resolution of 50 pc, was achieved for both the H I and CO observations. Our CO observations appear to have resolved GMCs in M31 similar in size and molecular hydrogen mass to those in the solar neighborhood of the Milky Way. These clouds are closely associated with H II regions and are active sites of star formation. The individual GMC complexes we detected appear to be made up of typically two or more large or intermediate-sized molecular clouds with no evidence for a population of small molecular clouds contributing to the observed emission. The velocity dispersion of the GMCs in the region observed is similar to that of GMCs in the solar neighborhood. Observations of the $J = 2 \rightarrow 1$ transition of CO were also obtained toward this region. Comparison of the intensities of the two CO transitions with model calculations suggest molecular hydrogen space densities and CO column densities similar to those of GMCs in the Milky Way. Our H I observations indicate that the GMCs we observed in M31 contain substantial amounts of atomic hydrogen gas which comprise about 30% of the total mass of a CO–H I cloud complex. The individual GMC complexes are gravitationally bound and have total (atomic and molecular) masses on the order of $10^6\ M_\odot$. The GMC–H I complexes appear to be local mass enhancements in a large H I spiral arm feature which otherwise consists of smoothly distributed H I gas. Between 15% and 20% of the total mass of the entire H I arm is estimated to be in molecular form.

In the region observed the distributions of atomic and molecular gas are clearly correlated in both space and velocity. The peak temperatures and integrated intensities of H I and CO emission are found to be linearly related, with the strongest CO emission ocurring in regions of strongest H I emission. The H I linewidths are typically around 25 km s^{-1} and are usually twice as wide as the CO lines observed along the same lines of sight. Hydrogen column density thresholds for H_2 and CO formation inferred from our data are very similar to corresponding values empirically determined for clouds in the Milky Way, and we find no evidence in our data to indicate that physical conditions in the M31 clouds differ in any substantive way from the physical conditions of local GMCs. The implication of these results for the formation and evolution of molecular clouds is discussed.

Subject headings: galaxies: individual (M31) — interstellar: molecules — nebulae: H II regions — radio sources: 21 cm radiation

I. INTRODUCTION

As a result of the recent development of large aperture telescopes for millimeter-wave and centimeter-wave spectral-line observations, investigation of the molecular and atomic components of the interstellar medium of nearby galaxies on the size scales of associations and giant molecular clouds is now possible. For example, recent CO observations have shown that the 45 m telescope of the Nobeyama Radio Observatory might be capable of resolving and mapping individual giant molecular clouds (GMCs) in M31 if well-sampled maps of star-formation sites are made (Ichikawa *et al.* 1985; Nakano *et al.* 1987; see also Boulanger *et al.* 1984). High-resolution studies of extragalactic molecular and atomic clouds can provide qualitatively new insights into important questions concerning their formation, evolution, and genealogical interrelation. Study of these issues has been complicated and inherently limited in our own Galaxy because of the disadvantaged point of view afforded by our internal location of observation. In particular, observations of H I gas associated with molecular clouds are made very difficult by an intense, pervasive, and often unrelated galactic background. These considerations motivated us to attempt a high-resolution, coordinated H I–CO study of an individual star-forming region in the nearby external galaxy M31. We used observations of the 21 cm spectral line of atomic hydrogen made with the VLA and observations of the $J = 1 \rightarrow 0$ transition of ^{12}CO made with the 45 m Nobeyama Radio Telescope to trace out the distribution of atomic and molecular gas with nearly identical high angular (15″ or 50 pc) and spectral (2.6 km s^{-1}) resolutions in a region designated A22/D118 in Hodge's atlas of M31 (Hodge 1981).

[1] Alfred P. Sloan Foundation Fellow.

The A22/D118 region was chosen for study because it contained a large, well-defined, OB association (A22 [Hodge 1981]), a prominent H II region (BA 289 [Baade and Arp 1964]), and a large dark cloud (D118 [Hodge 1981]), which were positioned in a sequential pattern, similar to that found for many star-forming complexes in the solar neighborhood (Elmegreen and Lada 1977). The entire region is located within a large atomic hydrogen feature which appears to be a segment of a spiral arm located 7 kpc from the center of M31 (Emerson 1976; Unwin 1980; Sofue and Kato 1981; Brinks 1984). CO emission has also been detected near this complex (Combes *et al.* 1977) indicating the presence of molecular clouds. These factors suggest that this region is a very active star-forming site.

From our observations we hoped to address some of the following broad questions. (1) What are the sizes and masses of molecular and atomic clouds in M31? (2) How do they compare with those in the Milky Way? (3) What is the relationship between atomic and molecular gas in an active star-forming region? (4) How do molecular clouds form and evolve in M31? In § II we discuss our observations and methods of data acquisition and calibration. In § III we present the results and analysis of the observations. We report that our observations have resolved individual giant molecular clouds in M31 whose sizes, masses, and physical conditions bear striking resemblance to GMCs in the solar neighborhood of the Milky Way. In § IV we discuss our H I and CO observations in the context of molecular cloud formation and evolution. The results of the paper are summarized in § V.

II. OBSERVATIONS

Observations of the 21 cm spectral line of atomic hydrogen in the direction of the A22/D118 region in M31 were obtained with the Very Large Array of the NRAO[2] at two different spatial resolutions. On 1984 September 11 this region was observed over an 8 hr period using the D array of the VLA to provide an angular resolution of 37″ at the center of the 30′ diameter field of view. On 1985 August 9 and 11 the region was observed over two 8 hr periods using the C array which provided an angular resolution of roughly 13″ in the center of a 30′ diameter field of view. For each observation 64 spectral line channels were used in conjunction with 18 antennas. The spectral resolution was 13 KHz, corresponding to a velocity resolution of 2.6 km s^{-1}. The coverage in the UV plane was excellent with the result that the strongest sidelobes were at 5% of peak power in each array. The point source 3C 48 was observed at least once every half-hour during both observing runs and was used for absolute flux calibration.

Observations of the ^{12}CO $J = 1 \rightarrow 0$ transition toward the A22/D118 region were made in 1985 February and March with the 45 m telescope of the Nobeyama Radio Observatory (NRO).[3] The angular resolution of these observations was 15″. The original spectra were obtained with 0.3 km s^{-1} resolution and then smoothed to a resolution of 2.6 km s^{-1} for comparison with the H I observations. The temperature scale for these CO observations has been calibrated to be approximately equal to T_R^* as measured on the NRAO 11 m telescope on Kitt Peak. In order to set this calibration, CO observations of Orion obtained with the NRO 45 m telescope during the same week as our CO observations of M31 (T. Hasegawa and I. Gatley 1985, personal communication) were compared to observations of Orion previously obtained with the NRAO 11 m telescope (Margulis and Lada 1985). The NRO observations consisted of a map of CO spectra obtained with 15″ spacing in a completely filled grid 2.°25 on a side centered on Orion KL. From these observations a single spectrum was constructed by a Gaussian convolution of the individual spectra to a 66″ beam. This convolved spectrum was then compared to a single CO spectrum of the same region made with the NRAO 11 m telescope. We found that in order to scale the convolved NRO spectrum to match the spectrum obtained at Kitt Peak, the raw temperatures obtained at NRO had to be multiplied by a factor of 3.2 in the core of the line and 4.2 in the line wings. With this scaling the peak temperature (T_R^*) of the line core measured with the 15″ beam of the NRO 45 m telescope toward Orion KL is 86 K. The different scaling factor for the line wings is most likely a result of the fact that the error patterns of the two telescopes couple differently to the emission in the line core. This is because the emission in the line wings, unlike that in the line core, arises from a region whose angular size (about 30″ in extent) is small compared to that of the error patterns of the two telescopes. For the M31 data we adopted a scale factor of 4.2, since the emission we observed arises from objects with angular sizes on the order of or smaller than that of the region of high-velocity flow in Orion. However, we note that none of the basic conclusions of this paper would be altered if the lower scale factor were adopted instead.

Observations of the CO $2 \rightarrow 1$ spectral line were also made in the direction of A22/D118 during 1985 May using the 12 m telescope of the National Radio Astronomy Observatory. These observations were obtained with an angular resolution of 33″. Spectra were obtained at two frequency resolutions, 500 KHz and 1 MHz, corresponding to velocity resolutions of 0.65 km s^{-1} and 1.30 km s^{-1}. Temperatures are expressed as T_R^* using the formalism of Ulich and Haas (1976) and Kutner and Ulich (1981).

Using a distance to M31 of 765 kpc (Sandage and Tammann 1968) projected spatial resolutions of the observations taken with the VLA were 140 and 50 pc in the D and C arrays, respectively. The projected spatial resolutions of the CO observations were 50 and 130 pc for the $J = 1 \rightarrow 0$ and the $2 \rightarrow 1$ transitions, respectively.

III. RESULTS AND ANALYSIS

a) The Angular Distribution of H I *and* CO *Gas*

Figure 1 shows the large-scale distribution of H I gas in the A22/D118 region of M31 alongside an optical photograph of the region taken from Hodge (1981). The contours represent the distribution of H I emission in a single channel at a velocity of -517 km s^{-1} as observed with the D array of the VLA. The H I emission appears concentrated in an elongated filament about 3.5×0.5 kpc in size. This feature appears to be a segment of a spiral arm located about 7 kpc from the center of M31. H I emission was detected over a velocity range of about 45 km s^{-1}, centered around -517 km s^{-1}, and H I maps at other velocities show the same overall morphology. The morphology of the H I filament is similar to that of the dark clouds, clusters, and associations in this region defined by Hodge (1981), which also lie in a line extending northeast to southwest more or less coincident with the H I gas. However, dark clouds

[2] The National Radio Astronomy Observatory is operated by Associated Universities Inc., under contract with the National Science Foundation.

[3] NRO, a branch of the Tokyo Astronomical Observatory, is a facility open for the general use by researchers in the field of astronomy and astrophysics.

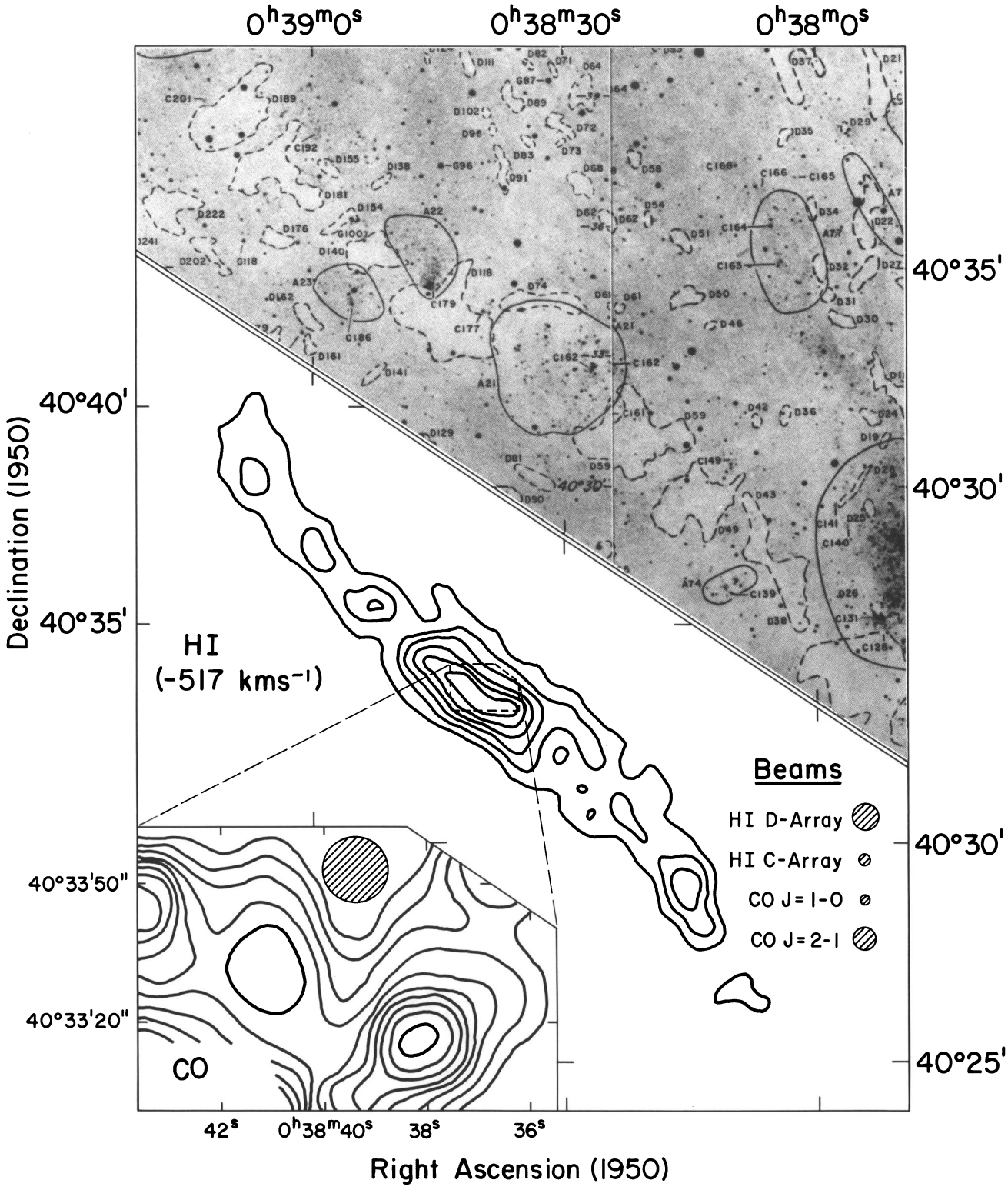

FIG. 1.—An optical photograph, the D array H I map and the NRO CO map of the A22-D118 region of M31 are shown together. The optical photograph is from Hodge (1981) and includes identification numbers for associations (A), clusters (C), and dark clouds (D) as cataloged by Hodge. The H I map is drawn on the same scale as the optical photograph and represents the distribution of H I emission in a single (2.6 km s^{-1} wide) channel at an LSR velocity of -517 km s^{-1}. The H I contours are equal spaced isoflux contours with intervals of 20 mJy, starting with 20 mJy. The insert is the NRO map of integrated CO intensity made of the region of brightest H I emission. In this map, the CO contours are measured in units of NRO antenna temperature (rather than T_R^*) and velocity, with contours having equal spacings of 0.4 K km s^{-1} starting with the 0.4 K km s^{-1} contour. The beam sizes for the various observations presented in this paper are also shown for comparison. The projected linear sizes of the CO $J = 1 \rightarrow 0$ and C array H I beams are both about 50 pc in diameter.

(e.g., D189, D181, D154, D140, D118, D59, D49, and D43) lie close to the center line of the H I filament, while the associations (e.g., A22, A23, A21, and A74) tend to be distributed with a greater dispersion around the center line. The strongest H I emission appears to arise from a region coincident with the dark cloud D118 about 250 pc southwest of the very bright H II region BA 289 which itself is located at the southwest boundary of the A22 OB association.

Figure 1 also shows a map of the ^{12}CO integrated intensity in the D118 region. The strongest CO lines were found to be well correlated with and centered within the distribution of strongest H I emission. The $\frac{1}{2}$ power extent of the CO emission is about half that of the H I emission in the region mapped. If the overall structure of the A22/D118 region is representative of the entire H I filament, then molecular gas may be concentrated near the center of this spiral arm segment along its entire length. Such a situation is suggested by the concentration of optical dark clouds along the spine of the filament and is also consistent with the CO maps made of this region with much lower angular resolution with the Bell Labs 7 m telescope (Linke 1981).

Our observations clearly resolve structure in the spatial distribution of integrated CO intensity. In particular, four peaks are evident in the CO map in Figure 1. Toward three of these peaks, CO emission is detected at more than one mapping position (i.e., they are extended with linear diameters in excess of 50 pc). The fourth peak, in the northwest corner of the map, shows emission at only one position (see Figure 4) and may not be significant. Therefore, from here forward we will confine our discussion to consideration of the three strongest CO peaks whose existence is confidently established. These three regions of enhanced CO emission have projected sizes and separations of about 100 parsecs. Apparently, our observations have resolved, for the first time, individual giant molecular cloud complexes in M31, similar in size to those in the Milky Way. The fact that two of the peaks in the CO distribution are clearly associated with optical H II regions (BA 292 and P248, see Fig. 2) indicates that massive stars are forming in these complexes. This strengthens the contention that we have resolved the molecular component of active star formation complexes in M31 similar to the GMCs in our own Galaxy. Figure 2 shows the CO map plotted alongside a map of the integrated H I emission of the same region constructed from our VLA observations made using the C array. When observed at the same angular resolution the H I distribution shows structure very similar to that of the molecular gas. Three enhancements in the H I integrated intensity are found at roughly the same locations as the CO complexes. However, the contrast in the H I map is considerably less than that in the CO map. Inspection of the maps shows that the peaks in the H I emission are only about 25% stronger than that of the general H I background, while the CO emission peaks are nearly an order of magnitude stronger than the general background of CO emission. As in the Milky Way, the molecular gas in M31 appears much more clumpy (on scales of 50 pc) than the H I gas. Close inspection of Figure 2 also reveals that the H I peaks, the CO peaks, and the positions of the H II regions are apparently offset from each other with separations between them on the order of 15″ (50 pc).

b) *The Velocity Structure of* H I *and* CO *Gas*

Figures 3 and 4 show the NRO CO spectra at each position we observed in the A22(Fig. 3)–D118(Fig. 4) region. In each figure the spectra are arranged according to the positions at which they were observed on the sky. For comparison, Figure 3 also includes a CO spectrum of the NGC 2264 molecular cloud as it would appear to the NRO telescope if it were located in M31. This spectrum was obtained by numerically convolving 1319 individual CO spectra observed over the cloud with 0.5 pc angular resolution (Margulis and Lada 1986) to a simulated beam with a half-power size of 50 pc. The NGC 2264 cloud is roughly 30 × 10 pc in size and contains a mass of molecular gas of about $3 \times 10^4\ M_\odot$. As can be seen our observations could have easily detected such a molecular cloud in M31 and most of the CO emission we detected from the A22/D118 region is at this level or considerably stronger. Figures 5 and 6 show the corresponding H I spectra observed with the C array of the VLA. The spatial and spectral resolutions of the CO and H I spectra in Figures 3–6 are virtually identical. In Table 1 we present the peak line strengths, LSR velocities at

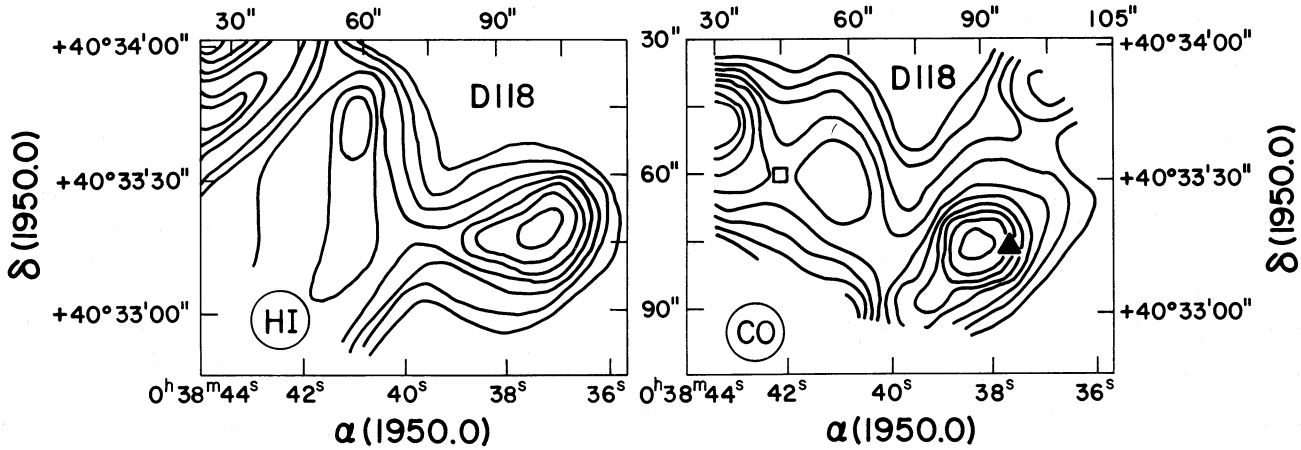

FIG. 2.—Maps of the distribution of integrated intensities of H I and CO emission from the D118 region obtained with the same angular resolution. The H I map was constructed from data obtained with the C array of the VLA. The contours are of integrated intensity measured in units of K km s^{-1} and are equally spaced at intervals of 200 K km s^{-1}, starting with the 2800 K km s^{-1} contour. Note that the lowest contour in the H I map has a value higher than that of the half-peak integrated intensity level (2200 K km s^{-1}) of the map. The CO map is basically the same as that in Fig. 1. Note that the lowermost contour is a factor of 10 lower than the peak integrated intensity in the map, indicating that the distribution of CO emission is much more clumpy than that of H I (see text for discussion). The positions of the optically identified H II regions P248 (Pellet *et al.* 1978) and BA 292 (Baade and Arp 1964) are indicated on the CO map by a square and a triangle, respectively.

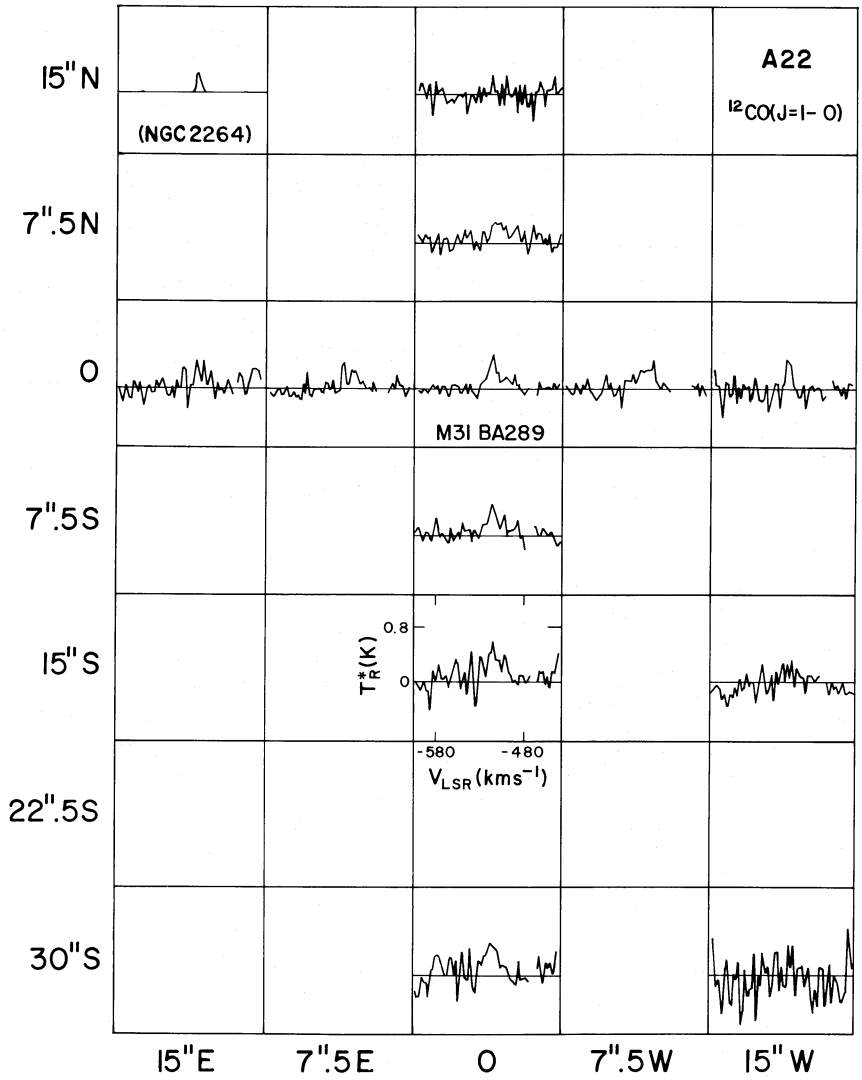

FIG. 3.—Observed $J = 1 \rightarrow 0$ spectra of CO obtained at NRO around the H II region BA 289. The spectra are arranged according to the positions at which they were observed on the sky. The positional offsets are in seconds of arc from the position of BA 289, which was the positional reference used for all our observations. Each spectrum is a plot of T_R^* vs. LSR velocity. In addition a spectrum of the NGC 2264 molecular cloud is also plotted as it would appear if observed in M31 by the NRO telescope. The NGC 2264 spectrum was constructed from observations made of this cloud with a 5 m telescope and convolved to the projected spatial resolution of the NRO 45 m telescope at the distance of M31. The line temperature of the convolved NGC 2264 spectrum is 0.3 K and the linewidth is 7.0 km s^{-1} (see text for discussion).

peak line strength, and the linewidth measured at half peak intensity for the spectra shown in Figures 3–6.

Figures 7 and 8 show the relationships between the peak temperatures and integrated intensities of the H I and CO profiles along the same lines of sight. For the 23 positions where both H I and CO emission were detected, both graphs show that there is a positive correlation between CO and H I brightness. The best linear fit through these data points in the peak temperature plot (Fig. 7) is given by: $T_R^*(\mathrm{CO}) = 5.0 \times 10^{-3}\ T_B(\mathrm{H\ I}) + 7.0 \times 10^{-3}$ K. The correlation coefficient is 0.51. The best linear fit through the corresponding data points in the integrated intensity plot (Fig. 8) is given by: $\int T_R^*(\mathrm{CO})dv = 3.0 \times 10^{-3} \int T_B(\mathrm{H\ I})dv - 1.82$ K km s^{-1} with a correlation coefficient of 0.54. The probabilities that these correlations could arise from the sampling of a parent distribution of randomly distributed data points are less than 2%. Since a large fraction of the data listed in Table 1 and plotted in Figures 7 and 8 consists of upper limits, it is useful to consider the effects of these *censored* data points on the derived correlations. In recent years statistical methods for treating univariate and multivariate data in which a portion of the data consists of upper limits have been introduced to astronomy (Feigelson and Nelson 1985; Isobe, Feigelson, and Nelson 1986). These methods were applied to the data set in Table 1 by Takashi Isobe (personal communication). Using the parametric EM algorithm described by Isobe, Feigelson, and Nelson (1986), the H I and CO peak temperatures and integrated intensities were found to be linearly related with a high degree of correlation. For the peak temperatures, the derived linear fit to all the data is given by: $T_R^*(\mathrm{CO}) = 6.1 \times 10^{-3}\ T_B(\mathrm{H\ I}) - 0.2$ K. For the integrated intensities the derived relation is: $\int T_R^*(\mathrm{CO})dv = 3.2 \times 10^{-3} \int T_B(\mathrm{H\ I})dv - 3.16$ K km s^{-1}. The Buckley-James method, also described by Isobe, Feigelson and Nelson, was applied to the data giving nearly identical results.

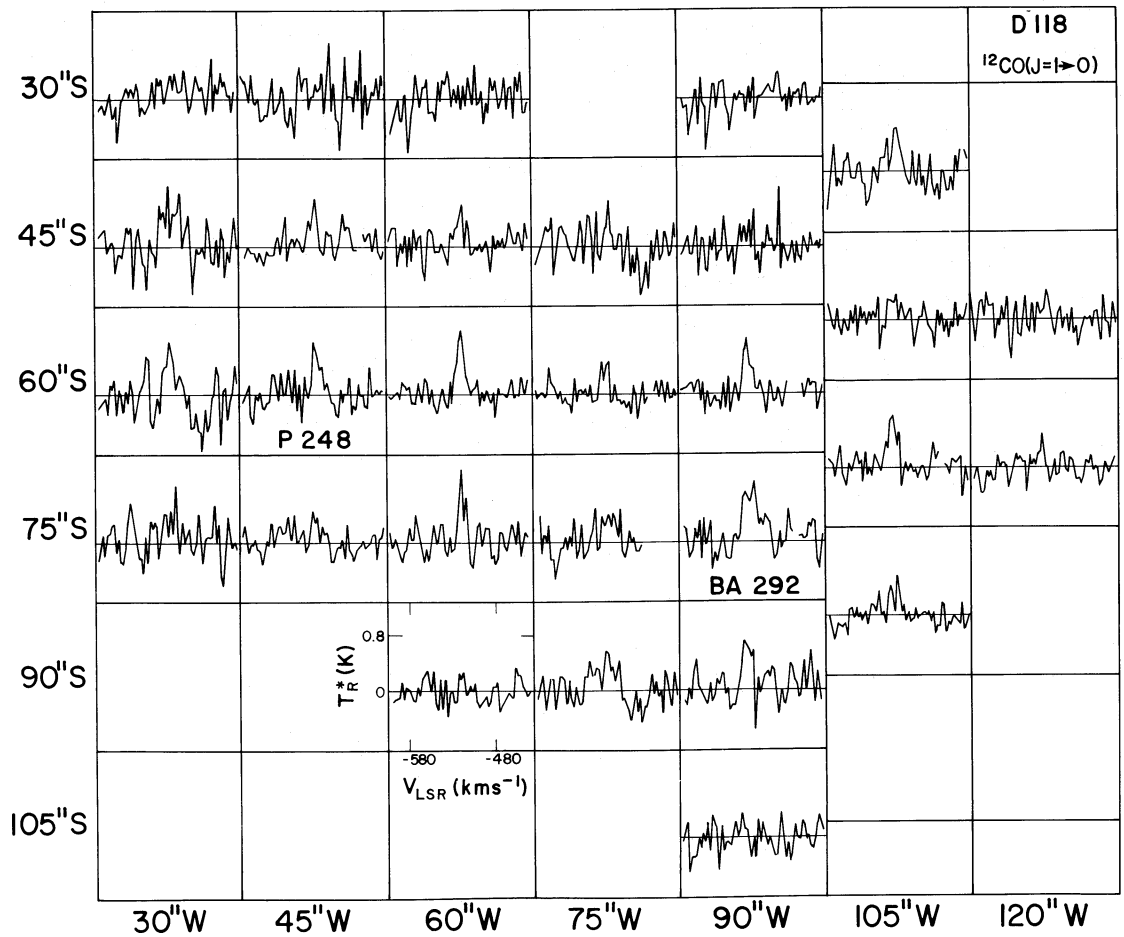

FIG. 4.—Observed CO spectra of the D118 region obtained with the NRO 45 m telescope. As in Fig. 1 the positions of the spectra are arranged according to their relative positions on the sky. The positional offsets are with respect to the position of BA 289.

In addition, the probability that these correlations could arise from sampling a parent distribution of randomly distributed data points was found to be less than 1% by a variety of methods. These results are remarkably similar to those derived above from consideration of the data set which excluded the upper limits. This suggests that the derived correlations are representative of the conditions at all the positions observed, even those where CO emission is yet to be detected.

As Table 1 shows the H I and CO emission are also correlated in velocity space. The mean of the difference between CO and H I peak velocities is -2.4 km s^{-1} (about one resolution element in velocity) with a dispersion of about 6 km s^{-1}. Even though the dispersion in the peak velocity difference is large, the CO lines are usually about a factor of 2 more narrow than the H I lines, so along a given line of sight the CO emission is always found over a velocity range within that from which H I emission arises. Figure 9 shows the CO and H I profiles observed at the same position toward the BA 292 cloud complex. Although the CO emission peaks 9.0 km s^{-1} lower in velocity than the H I emission, the velocity spread of the CO emission is well within that covered by H I gas. The LSR velocity dispersion (rms) of the CO line peaks in D118 is found to be about 4 km s^{-1}. This is probably a lower limit to the actual value since it refers to only the strongest line peaks observed at each position. From an average CO spectrum of the entire region (see below and Fig. 10), however, we estimate that the one-dimensional velocity dispersion of the clouds is less than or equal to 6 km s^{-1}. Thus, the velocity dispersion of the clouds in D118 is very similar to that ($\sim$5.7 km s^{-1}) of local galactic GMCs (e.g., Blitz 1985, 1987). Further comparison of the individual H I and CO profiles across our map also suggests that there may be more structure in the CO lines than observed in the H I profiles. In Figure 10 we plot average H I and CO spectra obtained by separately averaging all H I and CO spectra observed along lines of sight toward which CO emission was detected in a single observation. The average CO spectrum is more narrow than the average H I spectrum and contains three distinct velocity peaks. The average H I spectrum is considerably smoother in appearance than the CO profile. The signal-to-noise ratio was good enough in the average CO spectrum to enable a Gaussian deconvolution of the profile into three velocity components. The amplitudes, widths, and velocity centroids of the least-square fitted Gaussians are shown in Figure 10 and listed in the figure caption. The line widths of the three features (8.3 km s^{-1}, 5.9 km s^{-1}, and 3.3 km s^{-1}) are comparable to those expected for individual molecular clouds. This suggests that the structure and width of the observed CO line is due to the superposition of a discrete number of individual giant or moderate-sized molecular clouds. It is difficult to assess whether this particular least-squares fit to the spectrum is a unique representation of the data. Attempts to fit the data with other combinations of

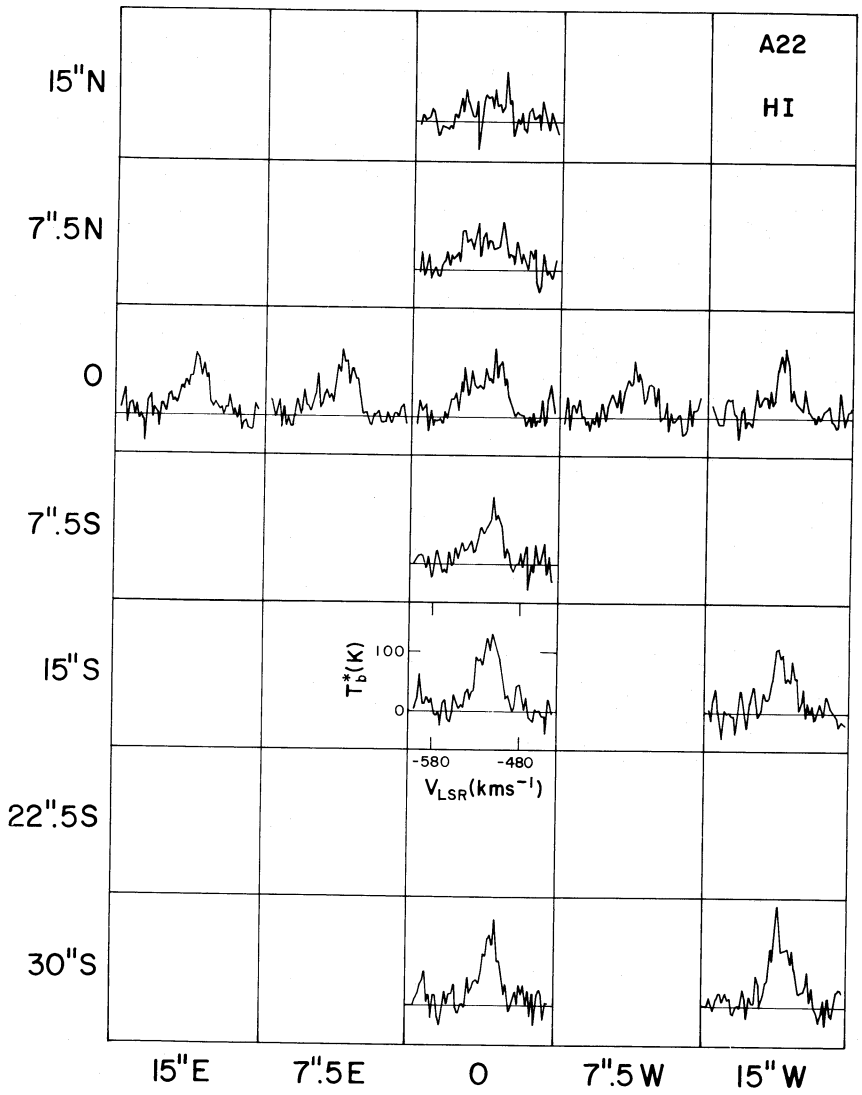

FIG. 5.—Observed H I spectra obtained with the C array of the VLA along the same lines of sight as the CO spectra in Fig. 3. These H I spectra were obtained with the same spatial and velocity resolutions as the CO observations.

Gaussian functions, for example, two narrow components and a broad pedestal, were unsuccessful. However, a two-Gaussian fit matched the data with residuals only slightly worse than the three-Gaussian fit adopted here. This is not surprising since the weakest component in the adopted fit is only marginally present (see Fig. 10). In any event, there appears to be no evidence for significant emission from a uniformly distributed population of small (i.e., $M \leq 10^4\ M_\odot$) or very small (i.e., $M \leq 10^2\ M_\odot$) molecular clouds within the volume of the D118 region we observed. Emission from such clouds is thought to dominate the CO emission profiles observed in M31 with smaller telescopes, because the larger beam sizes and resulting dilution reduce the relative contribution of the less pervasive GMCs to the observed spectra (Boulanger, Stark, and Combes 1981; Blitz 1985). In order to estimate the extent to which a distributed population of small clouds contributes to the emission from this region we constructed an average CO and an average H I spectrum for all positions in Figure 3 without detectable CO emission. These average spectra are also shown in Figure 10. Within the noise there is no evidence for significant emission from a distributed population of small clouds in the average CO spectrum from positions without detectable CO emission in a single scan. The upper limit to the line emission from these positions is $T_R^* \leq 0.2$ K. This limit is consistent with the intensity expected from small clouds in a 15″ beam pointed at M31 (Blitz 1985) and does not necessarily rule out their presence in this region. However, our observations indicate that such clouds contribute at most a small fraction (i.e., < 25%) to the total molecular mass of the region. This is similar to the situation in the solar neighborhood of the Milky Way where small high-latitude molecular clouds are found to consititute only about 10% of the total molecular mass (Magnani, Lada, and Blitz 1986) and GMCs dominate the total molecular mass. The average spectra in Figure 10 again clearly show that the spatial contrast in CO emission is significantly greater than that in H I emission in the D118 region. This strengthens the notion that the CO emission arises from individual giant molecular cloud complexes, while the atomic gas is contained in a more smoothly distributed component. However, the integrated intensity from the H I in the CO emitting regions is a factor of 1.4 stronger than that in the non–CO emitting regions indicating a significant enhancement

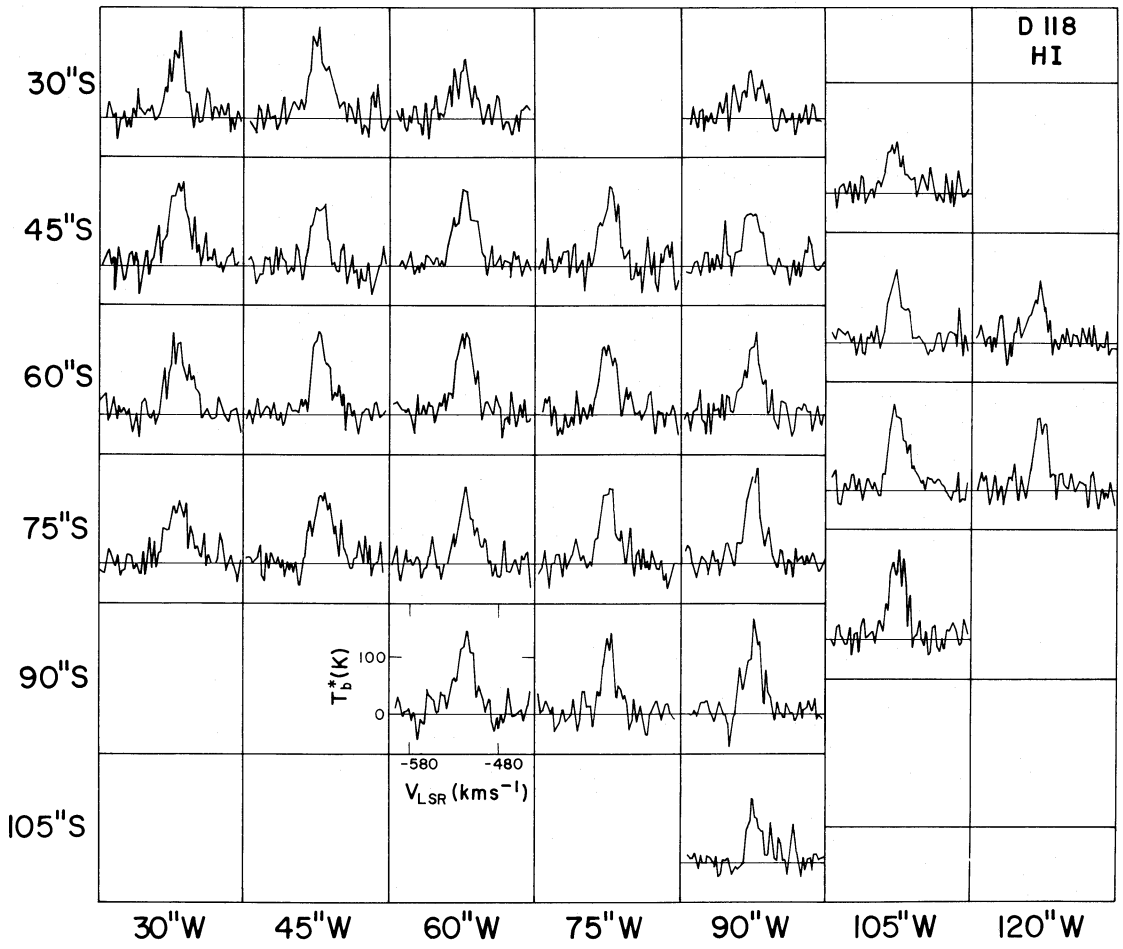

FIG. 6.—Observed H I spectra obtained with the C array of the VLA along the same lines of sight as the CO spectra in Fig. 4

of H I along the lines of sight to the molecular cloud complexes.

c) Column Densities and Masses of the H I *and* CO *Gas*

Using our spectra we were able to derive column densities of atomic and molecular hydrogen at each position where an emission line was detected. From the H I spectra column densities of *atomic* hydrogen were derived from (Spitzer 1978):

$$N(\mathrm{H}) = \int_{\mathrm{line}} 1.82 \times 10^{18} T_B(\mathrm{H\ I}) dv \ \mathrm{cm}^{-2} \qquad (1)$$

From the CO spectra column densities of *molecular* hydrogen were derived from (Bloemen *et al.* 1986; Sanders, Solomon, and Scoville, 1984):

$$N(\mathrm{H_2}) = \int_{\mathrm{line}} 2.8 \times 10^{20} T_R^*(\mathrm{CO}) dv \ \mathrm{cm}^{-2} \qquad (2)$$

The column densities derived in this manner are listed for each position in Table 1. The statistical uncertainties in these determinations are on the order of 10% and 15% for the strongest H I and CO lines, respectively. The overall uncertainties in these column densities are dominated by systematic errors which are difficult to estimate. The accuracy of the estimates largely depend on the reliability of the assumptions used in the derivations of equations (1) and (2). For the H I column density we assumed that the H I emission was optically thin, and since we see little evidence for self-absorption, this is probably a reasonable assumption. The derived molecular hydrogen column densities are considerably more uncertain that the atomic hydrogen column densities. This is because the molecular hydrogen densities are not derived directly from observations of the molecular hydrogen itself. Instead, observations of CO are used as a surrogate. The CO–H_2 calibration used in equation (2) has been derived independently from comparison of ^{12}CO emission directly with observations of gamma rays (Bloemen *et al.* 1986) and indirectly with visual extinction (e.g., Sanders, Solomon, and Scoville 1984) toward many galactic molecular clouds. The uncertainties in this calibration have been extensively discussed elsewhere (e.g., Bloemen *et al.* 1986; van Dishoeck and Black 1987) and for a given molecular cloud complex in the galaxy, column densities of molecular hydrogen derived using equation (2) are good to about a factor of 2. A similar level of confidence in this calibration applies to M31 only if the CO-to-H abundance ratio there is the same as that in our own Galaxy. As we will argue later, our $J = 2 \rightarrow 1$ CO observations suggest that this is probably a reasonable assumption.

If equations (1) and (2) are appropriate for deriving column densities, then the observed correlation between the integrated intensities of H I and CO (Fig. 8) implies a correlation between the molecular and atomic hydrogen column densities. Using equations (1) and (2), we transform the equation describing the

TABLE 1

H I AND CO SPECTRAL-LINE PARAMETERS AND COLUMN DENSITIES

	HI				CO			
Position[a] (arc seconds)	T_B^b (K)	Velocity[c] (km s^{-1})	ΔV(FWHP) (km s^{-1})	N(HI)[d] (x 10^{21}cm^{-2})	T_R^{*b} (K)	Velocity[c] (km s^{-1})	ΔV(FWHP) (km s^{-1})	N(H_2)[d] (x 10^{21}cm^{-2})
15E,0	107±24	−512	28	6.4±0.4	<0.41	—	—	<2.1
7.5E,0	115±20	−514	26	6.4±0.3	0.38±0.07	−514	18	1.4±0.1
0,15N	<60	—	—	<0.9	<0.32	—	—	<1.6
0,7.5N	81±22	−501	51	6.9±0.5	<0.41	—	—	<2.1
0,0	116±17	−509	53	7.4±0.4	0.50±0.04	−514	12	2.2±0.1
0,7.5S	115±20	−509	29	5.3±0.3	0.46±0.09	−514	8	1.8±0.1
0,15S	130±24	−509	31	7.8±0.4	0.62±0.14	−514	30	3.3±0.3
0,30S	146±28	−506	21	6.2±0.4	0.49±0.22	−514	19	2.7±0.4
7.5W,0	97±23	−517	35	4.9±0.4	0.45±0.07	−501	18	2.3±0.1
15W,0	108±19	−512	16	5.0±0.2	0.45±0.07	−518	8	1.1±0.1
15W15S	111±30	−517	28	5.7±0.5	<0.36	—	—	<1.8
15W30S	174±24	−517	28	8.2±0.4	<0.86	—	—	<4.3
30W30S	143±23	−512	18	5.8±0.3	<0.81	—	—	<4.1
30W45S	143±26	−509	23	8.1±0.4	0.89±0.22	-520	25	3.7±0.5
30W60S	137±25	−519	30	5.9±0.4	0.79±0.09	−520	13	2.8±0.1
30W75S	107±30	−511	34	6.1±0.5	<0.81	—	—	<4.1
45W30S	151±30	−519	26	7.2±0.4	<0.90	—	—	<4.5
45W45S	115±30	−512	21	5.8±0.4	0.71±0.17	−520	11	1.7±0.3
45W60S	142±20	−519	23	6.3±0.3	0.80±0.21	−522	12	2.4±0.3
45W75S	121±29	−512	38	6.3±0.5	<0.69	—	—	<3.5
60W30S	97±19	−519	28	4.0±0.3	<0.86	—	—	<4.3
60W45S	130±19	−522	31	6.9±0.3	0.63±0.19	−520	13	1.9±0.3
60W60S	140±24	−517	26	6.7±0.4	0.97±0.14	−520	9	2.7±0.2
60W75S	138±24	−517	18	6.5±0.3	1.10±0.21	−520	9	2.1±0.3
60W90S	139±32	−514	21	6.4±0.4	<0.32	—	—	<1.6
75W45S	140±30	−524	25	5.5±0.4	<0.86	—	—	<4.3
75W60S	120±28	−522	21	5.6±0.4	0.50±0.12	−528	10	1.2±0.2
75W75S	130±24	−519	17	6.3±0.3	<0.62	—	—	<3.1
75W90S	137±20	−517	15	4.2±0.2	0.59±0.12	−523	11	2.2±0.2
90W30S	81±23	−527	38	3.6±0.4	<0.54	—	—	<2.7
90W45S	92±24	−527	26	4.8±0.4	<0.90	—	—	<4.5
90W60S	139±24	−519	21	5.8±0.3	0.84±0.16	−528	8	2.4±0.2
90W75S	164±24	−517	18	6.9±0.3	0.89±0.27	−520	18	5.0±0.5
90W90S	162±17	−522	16	5.6±0.2	0.72±0.21	−530	15	2.6±0.4
90W105S	110±14	−522	18	4.2±0.2	<0.64	—	—	<3.2
105W37.5S	88±27	−525	23	4.2±0.4	0.67±0.23	-522	8	1.8±0.3
105W52.5S	124±20	−525	16	4.8±0.2	<0.58	—	—	<2.9
105W67.5S	148±18	−527	25	7.2±0.3	0.76±0.15	−528	13	2.7±0.2
105W82.5S	156±26	−519	21	6.2±0.3	0.59±0.09	−523	14	1.8±0.2
120W52.5S	104±24	−525	16	4.0±0.3	<0.47	—	—	<0.7
120W67.5S	126±28	−527	18	5.1±0.3	0.51±0.12	−523	5	1.1±0.1

[a] Position relative to BA 289 $\alpha(1950) = 00^h38^m46^s2$ $\delta(1950) = 40°34'32''$.
[b] Peak intensity in profile. Quoted errors are 1 σ; upper limits are 3 σ values.
[c] LSR velocity at peak intensity.
[d] Derived column densities: quoted errors are 1 σ; upper limits were calculated assuming a line width which was the average line width of either the observed H I or CO profiles as appropriate.

best linear fit through the integrated intensities (excluding upper limits) to derive

$$N(H_2) = 0.46N(\text{H I}) - 5.09 \times 10^{20} \text{ cm}^{-2} . \quad (3)$$

The correlation between molecular and atomic hydrogen column densities is intriguing because it may provide important clues concerning the genealogical relationship and evolutionary histories of atomic and molecular clouds in M31. For one thing, equation (3) (and more significantly the empirical correlation between CO and H I integrated intensities) suggests that the H I and CO emission we observe are in some way physically related. In particular, in spite of the highly inclined nature of the disk, there does not appear to be a significant contribution to the observed H I emission from interarm H I gas along the line of sight and it is likely that the bulk of the observed H I emission, like the CO emission, originates in the H I arm. Indeed, if we adopt a model for the disk in which the H I scale height is 100 pc, the arm width 400 pc, the H I arm-interarm density contrast factor is equal to 6 and the face on H I interarm column density is that determined by Sofue and Kato (1981; i.e., 4×10^{20} cm^{-2}); then we predict that 80% of the observed H I emission would originate in the arm. Furthermore, equation (3) and close correspondence of H I and CO emission in Figure 2 suggest that on scale sizes of 100 pc molecular clouds exist in regions where a significant fraction of the neutral gas is in atomic form. If molecular clouds form from atomic clouds, then the conversion of atomic gas to molecular gas is never complete on the size scales of the molecular complexes (50–100 pc).

The fact that equation (3) appears to have a negative y-intercept suggests that there is a threshold in H I column density below which CO emission cannot be detected. The presence of such a threshold has been suggested in other studies of M31 (Nakano *et al.* 1987). If equations (1)–(3) are valid, this threshold could be interpreted as a critical column density below which hydrogen molecules cease to exist. Equa-

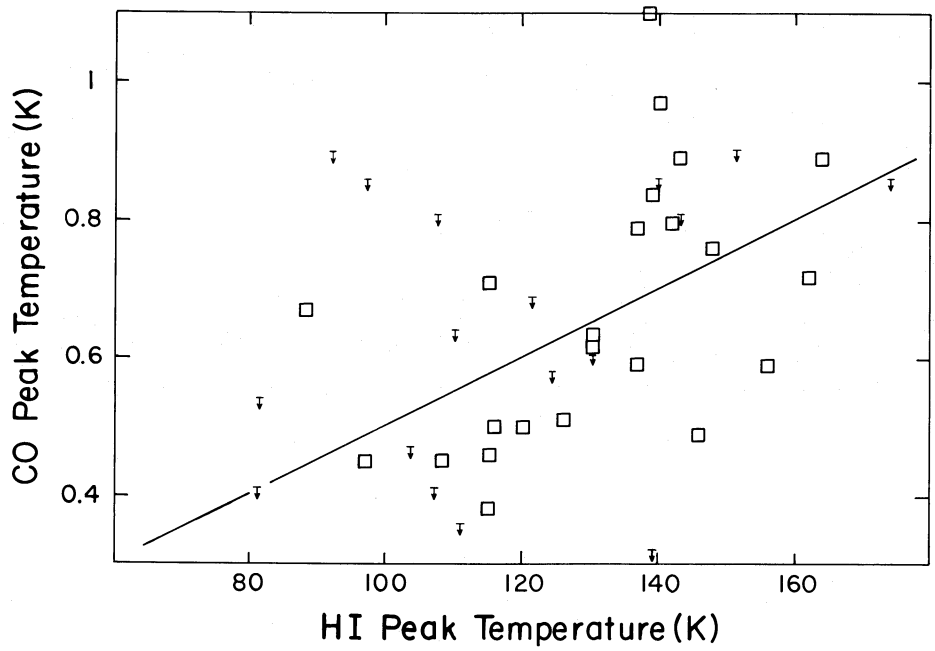

FIG. 7.—Observed correlation between CO and H I peak temperatures from the observations presented in Figs. 3–6. Open squares correspond to positions where both CO and H I emission lines were detected. Other points represent upper limits resulting from the lack of detectable CO emission. The line drawn through the points is the best-fit, least-squares linear relation for those positions for which both CO and H I emission was detected (i.e., *open squares*).

tion (3) suggests that this threshold occurs at $N(\mathrm{H}) \approx 10^{21}$ cm^{-2}. The existence of such a threshold is not surprising since molecular hydrogen cannot survive destruction by photodissociation from background starlight unless column densities of H_2 are large enough to permit self-shielding. In our Galaxy this self-shielding threshold is empirically determined to be $N(\mathrm{H}) \approx 6 \times 10^{20}$ cm^{-2} (Savage *et al.* 1977; Savage and Mathis 1979). The close correspondence between these two values is probably fortuitous, given the uncertainties in the M31 data. The value we derived for M31 is most likely an upper limit to the actual value. Indeed, we would expect that the empirical relation between H I and CO integrated intensities to become very nonlinear at column densities $\leq 10^{21}$ cm^{-2}, since the CO molecule requires much larger column densities than H_2 to shield itself against photodestruction (e.g., van Dishoeck and Black 1987). Therefore, the linear extrapolation of our

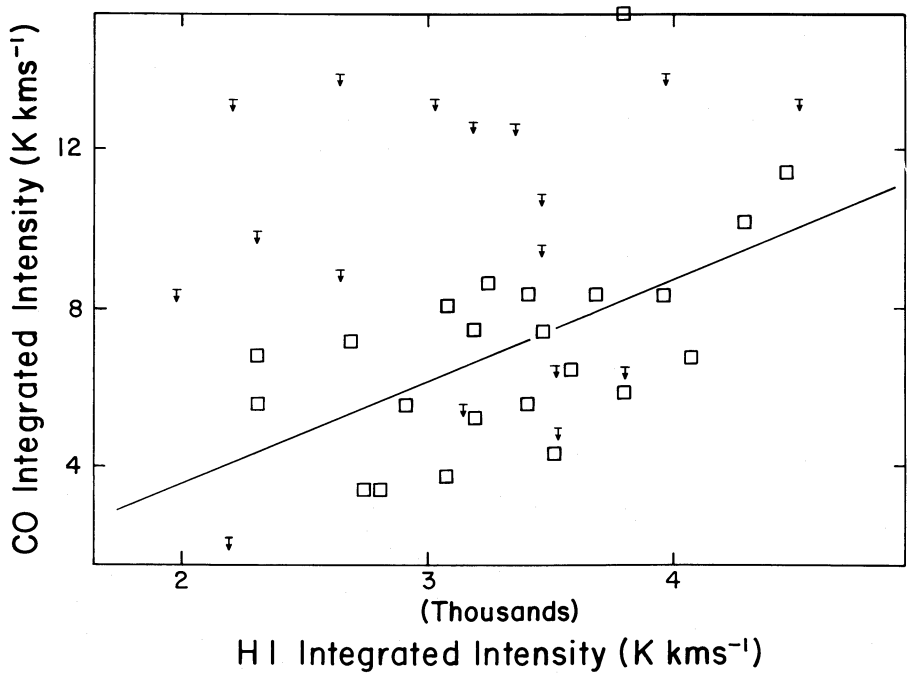

FIG. 8.—Observed correlation between CO and H I integrated intensities from the observations presented in Figs. 3–6. The symbols are the same as in Fig. 7. The line drawn through the data is the best-fit, least squares linear relation for those positions for which both CO and H I emission was detected (i.e., *open squares*).

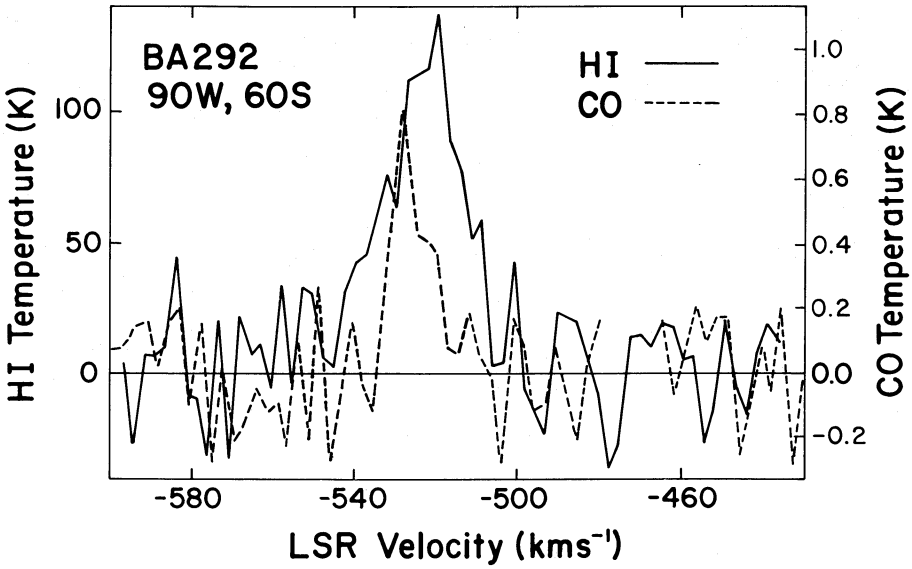

FIG. 9.—CO and H I emission spectra observed toward the molecular cloud associated with BA 292 with the same spatial and spectral resolution are plotted together for comparison. Note that the CO line is about half as wide as the H I profile, a characteristic typical of many profiles at the locations where both lines were detected.

observed correlations to low hydrogen column densities should be considered with some caution. An independent and perhaps more appropriate estimate of a threshold for CO detectability in M31 can be derived from the data presented in Figure 10. From these spectra we find that at positions without CO emission in D118 the average atomic hydrogen column density is about 5×10^{21} cm^{-2}. In our Galaxy CO becomes detectable when the total hydrogen column density exceeds $2\text{–}5 \times 10^{21}$ cm^{-2} (Lada and Blitz 1987). Although it again may be fortuitous, the close agreement between the threshold derived from our data and that for galactic molecular clouds suggests that the pertinent conditions (i.e., interstellar radiation field, gas-to-dust ratio, CO-to-H abundance, cloud geometry) in this region of M31 may not be all that different from the corresponding ones in the solar neighborhood.

From the spectra in Figure 10, we also find that the average *molecular* hydrogen column density toward all positions at which CO emission was detected is about 2×10^{21} cm^{-2}. Along the same lines of sight the average *atomic* column density is about 7×10^{21} cm^{-2}. Thus at the positions of the molecular clouds the total amount of hydrogen in all forms is about a factor of 2 or greater than it is in positions in the spiral arm without detectable CO clouds. Clearly, the molecular cloud complexes in D118 represent regions of enhanced total gas mass compared to the spiral arm in general.

It is useful to derive and compare masses for the various components of the D118 region. In Table 2, we list the derived atomic, molecular, and total gas masses for the entire D118 region and two of the giant cloud complexes within it. Within the boundaries of the maps in Figure 2, about 25% of the total gas mass is in the form of molecular hydrogen. For the H I filament or arm as a whole we estimate that only about 15%–20% of the total gas mass is in the form of molecular hydrogen. The H I emission in the arm is extended over a region twice as large as that of the CO emission, and even though the H I column density there is about a factor of 2 lower than in the region of the CO map, the total H I mass is comparable. For comparison, in the solar neighborhood of our own Galaxy molecular hydrogen accounts for about 17% of the total gas mass (e.g., Elmegreen and Elmegreen 1987). It is possible that we have underestimated the true abundance of molecular hydrogen throughout this spiral arm feature, since we derived molecular hydrogen masses for only those clouds with detectable CO emission. A significant fraction of the H I emission at positions or velocities that did not exhibit detectable CO emission may come from small clouds which contain substantial amounts of molecular hydrogen but whose CO abundances are too low to emit detectable millimeter-wavelength CO lines. The ζ Oph cloud being an example of such a cloud in our own Galaxy (van Dishoeck and Black 1987).

The sizes and masses of the molecular cloud complexes

TABLE 2

CLOUD MASSES

Cloud Designation	Radius	$M_{H_2}(M_\odot)$	$M_{HI}(M_\odot)$	$M_{H_2+HI}(M_\odot)$	$M_{total}(M_\odot)$
D118 region (Fig. 2)	125 pc	1×10^6	3×10^6	4×10^6	5.6×10^6
BA 292	48 pc	5×10^5	6×10^5	1×10^6	1.4×10^6
P248	57 pc	4×10^5	5×10^5	9×10^5	1.3×10^6
BA 289	25 pc	3×10^5	6×10^5	9×10^5	1.3×10^6

NOTE.—Total mass includes correction factor of 1.4 for presence of helium and heavier elements. The H I masses listed are those calculated for all the observed H I gas along the line of sight to the individual clouds.

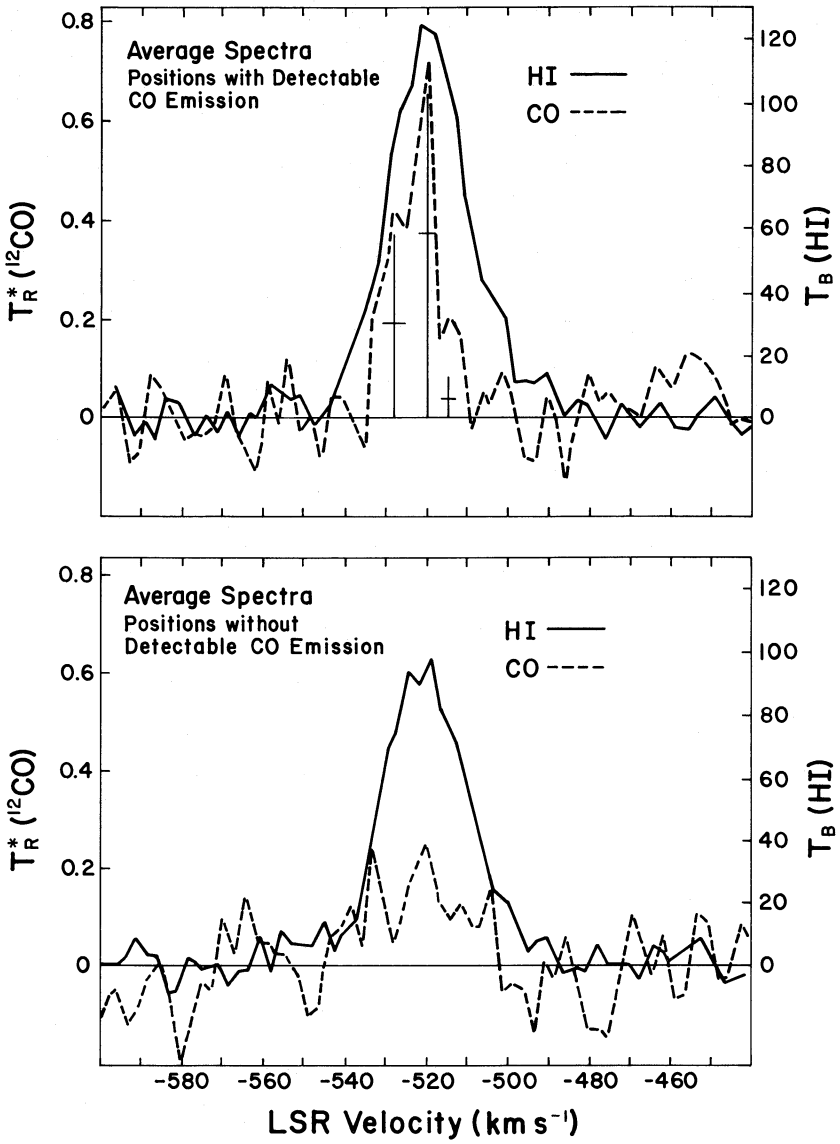

FIG. 10.—Average CO and H I spectra obtained by averaging all the H I and CO data obtained toward the D118 region at positions where CO was detected in Fig. 3 (*top box*) and positions where no CO lines were detected in Fig. 3 (*bottom box*). The average CO profile from positions where CO was detected has well-defined structure in velocity which can be successfully modeled by a Gaussian deconvolution of the line into three components. The amplitudes, positions, and widths of three Gaussian functions which represent the best three-Gaussian plus linear baseline least-squares fit to this spectrum are represented by crosses in the figure. The amplitudes, LSR velocities and widths of these lines were found to be: 0.37 ± 0.04 K, 0.72 ± 0.04 K, 0.07 ± 0.11 K, -530.6 ± 0.73 km s^{-1}, -521.2 ± 0.51 km s^{-1}, -515.0 ± 1.32 km s^{-1}, 8.3 ± 1.5 km s^{-1}, 5.9 ± 2.5 km s^{-1} and 3.3 ± 1.7 km s^{-1}, respectively. The average H I emission profile is both wider and smoother in shape than the CO profile. The average H I profile from positions without detectable CO is essentially structureless and has an integrated brightness about a factor of 1.4 less than the average H I profile from positions with detectable CO emission.

associated with the H II regions BA 292 and P248 are similar to those of GMCs in our Galaxy. The CO line widths are larger than one might expect from a single GMC, but as discussed earlier the observed profiles are probably the result of a superposition of more than one large cloud along the line of sight. But are the clouds in each complex indeed physically related? From the total line widths and sizes of the CO complexes we can investigate the extent to which these complexes are gravitationally bound by application of the virial theorem. Considering only the molecular gas we find the virial masses of the two complexes to be $1 \times 10^6\ M_\odot$ and $8 \times 10^5\ M_\odot$ for the BA 292 and P248 complexes, respectively. These values are within a factor of 2 of the masses calculated independently from equation (2) and strongly suggest that the entire molecular component of the complexes is gravitationally bound and that the individual molecular clouds in each complex are physically related. The virial masses estimated for the individual clouds in each complex are on the order of $2\text{–}3 \times 10^5\ M_\odot$, and these clouds are certainly bound, and perhaps even in virial equilibrium.

It is of course of interest to consider the relation of the atomic gas to the complexes. As can be seen in Table 2, the H I masses are comparable to the molecular masses along the lines of sight to the molecular clouds. However, the H I lines have larger line widths and likely arise from a larger volume than that containing the CO clouds. Thus it may not be reasonable

to attempt to associate all the H I gas observed toward the molecular clouds with the complexes themselves. As discussed earlier, the atomic hydrogen column density away from the molecular clouds is an appreciable fraction of the atomic hydrogen density observed toward the clouds. From Figure 10 we estimate a lower limit to the H I associated with each complex to be about 30% of the total observed H I column density. In which case the corresponding atomic hydrogen mass would be about $2 \times 10^5\ M_\odot$ for each complex, which is about half the molecular mass in each complex. We expect that in this case the associated atomic gas covers a velocity range similar to that of the CO gas and is thus clearly bound to the individual complexes. In any event, our data indicate that the molecular cloud complexes in D118 contain significant amounts of atomic gas. On the order of 30% of the total mass of a bound giant molecular complex in this region of M31 may be composed of atomic gas. Similar sized, bound molecular complexes have been observed in a spiral arm feature about 11 kpc from the center of M31 by Boulanger *et al.* (1984). From comparison with H I observations, these authors estimated that atomic hydrogen accounted for about 40% of the total mass of the two GMC complexes they studied. It is useful to compare these results to observations of galactic molecular clouds. Atomic hydrogen halos are known to exist around giant molecular clouds (e.g., Wannier, Lichten, and Morris 1983); however, their masses are difficult to estimate because of confusion with background H I emission. In a few cases where such confusion is minimized, reasonable H I mass estimates have been obtained. For the Orion molecular cloud complex about 15% of the total gaseous mass is in the form of atomic hydrogen (Gordon 1970; Maddalena *et al.* 1986), while in W3-4 and the Rosette complexes about 50% of the total gas mass is atomic in form (Hasegawa, Sato, and Fukui 1983; Lada *et al.* 1978; Blitz and Thaddeus 1980). These values are comparable to those which we obtain for the cloud complexes in D118 in M31.

d) $J = 2 \rightarrow 1$ CO Observations: Physical Conditions in the Molecular Gas

In order to investigate the physical conditions in the molecular gas in the D118 region we obtained an observation of the $J = 2 \rightarrow 1$ transition of CO toward this region. This observation was made toward the P248 cloud complex with the 12 m telescope on Kitt Peak which has a beam size of 33″ at the $J = 2 \rightarrow 1$ observing frequency. In order to make a useful comparison with the $J = 1 \rightarrow 0$ observations, we constructed a single $J = 1 \rightarrow 0$ spectrum from the NRO data by convolving the individual spectra in the D118 region to a synthetic 33″ beam centered at the same position as the $J = 2 \rightarrow 1$ observation. In Figure 11 we show the convolved $J = 1 \rightarrow 0$ spectrum along with the $J = 2 \rightarrow 1$ spectrum. The line widths (FWHI) of the two profiles are the same, 7 km s^{-1}. However, the $J = 1 \rightarrow 0$ profile exhibits structure on its high-velocity side, indicating the existence of an additional velocity component which is not visible in the more noisy $J = 2 \rightarrow 1$ spectrum. The temperature scales in Figure 11 are set to the T_R^* scale as measured at NRAO. For comparison of the two line strengths, however, it is more appropriate to use a brightness temperature T_B (or equivalently T_R in the formalism of Kutner and Ulich 1981) of the emission lines than a T_R^* since the coupling of the source intensity distribution to the telescope beams is different for the two telescopes at the two different frequencies. To determine brightness temperatures we need to know the angular distributions of source brightness and the antenna response functions of both telescopes. In both cases the telescope error patterns contain a nonnegligible fraction of the observed power, but in neither case do we have requisite knowledge of the structure of the error patterns to permit a detailed deconvolution. However, we do know that the molecular clouds in D118 are small compared to the sizes expected for the telescope error patterns so the cloud brightness distributions may not be expected to couple that strongly to the error patterns. Consequently, we may be able to estimate *main beam* brightness temperatures for the two spectra from the T_R^* temperature scales with knowledge of the coupling efficiency η_c (Ulich and Haas 1976; Kutner, Mundy, and Howard 1984) for a source which just fills the main beam. For the $2 \rightarrow 1$ observations $\eta_c = 0.48$ for a source which just fills the main beam; for the $J = 1 \rightarrow 0$ observations we estimate that $\eta_c = 0.70$ from comparison of our convolved spectrum of Orion with 11 m observations (see § II). Since the spectra in Figure 11 are convolved to the same beam size, the ratio of *main beam* brightness temperatures will equal the ratio of source brightness temperatures if we assume that the source sizes at the two frequencies are the same. With the appropriate corrections made we find that the ratio of the $J = 1 \rightarrow 0$ to $J = 2 \rightarrow 1$ brightness temperatures is 3.4.

In order to interpret the ratio of brightness temperatures derived above in terms of physical conditions in the molecular gas, we calculated the expected ratios of these transitions in a numerical model (provided by Philip Maloney). The model assumed statistical equilibrium and a plane parallel slab geometry and calculated the peak line temperatures from the nine lowest rotational transitions of CO as a function of kinetic temperature, CO column density, molecular hydrogen number density, and CO line width. Assuming a cloud kinetic temperature of 10 K and a line width of 10 km s^{-1} models were calculated for a wide range of CO column density and molecular hydrogen number density. The results of these calculations are shown in Figure 12 where we plot contours of equal CO $J = 1 \rightarrow 0$ brightness temperatures and $J = 1 \rightarrow 0/J = 2 \rightarrow 1$ line ratios. Considering the noise in the observed spectra we estimate the appropriate ratio of line temperatures is likely to be between 3.0 and 3.8, while the average $J = 1 \rightarrow 0$ brightness temperature is likely to be between 2 and 6 K depending on how well the cloud fills the convolved beam (for comparison the average brightness temperature of the NGC 2264 molecular cloud is 4 K, Margulis and Lada 1986). From the figure and the calculations we find that the range in observed parameters can be produced by models with hydrogen number densities between roughly 10 and 1000 cm^{-3} and CO column densities between 10^{17} and 3×10^{18} cm^{-2}. These number densities and column densities are similar to those one would expect from average properties of galactic molecular clouds and suggest that basic properties, such as the CO to H ratio, the number densities, temperature, etc., of the molecular clouds in the D118 region of M31 are similar to those of molecular clouds in the Milky Way.

IV. DISCUSSION

Our CO observations appear to have resolved extragalactic GMCs similar in size and mass to those in the solar neighborhood of the Milky Way. As in the Milky Way, these clouds are closely associated with H II regions and are active sites of star formation. Our H I observations indicate that these GMCs contain substantial amounts of atomic hydrogen gas which

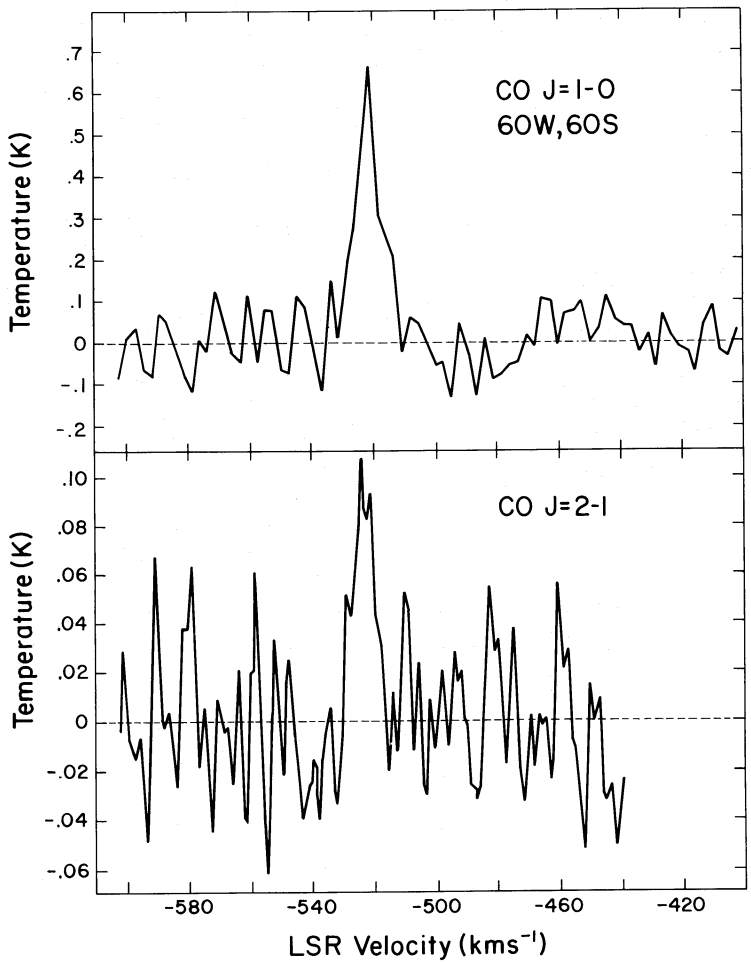

FIG. 11.—Observed $J = 1 \rightarrow 0$ and $J = 2 \rightarrow 1$ spectra from a position toward the P248 molecular cloud. The $J = 1 \rightarrow 0$ spectrum has been constructed by convolving appropriate NRO spectra to the same beam size as the $J = 2 \rightarrow 1$ spectrum (i.e., 33″) which was obtained with the NRAO 12 m telescope. The temperature scales for both spectra are T_R* equivalent scales.

comprise about 30% of the total mass of the cloud complex. The complexes are gravitationally bound and represent localized mass enhancements in a large H I spiral arm feature, 7 kpc from the center of M31. The molecular component of each complex appears to be made up of typically two or more large or intermediate-sized molecular clouds. The velocity dispersion of the CO clouds is similar to that of GMCs in the solar neighborhood. From the H I and CO observations we find no evidence to indicate that the physical conditions in these cloud complexes is different in any substantive way from the physical conditions in local GMCs in our Galaxy. Recently, higher resolution CO observations of this region have been obtained with the millimeter-wave interferometer at Owens Valley Radio Observatory. Vogel, Boulanger, and Ball (1987) synthesized a minute of arc field of view centered on BA 292 with a projected spatial resolution equal to about 25 pc. They detected CO emission from the BA 292 cloud over a region about 60 × 20 pc in extent. The CO emission measured by the interferometer was centered at an LSR velocity of about −530 km s^{-1} and observed over a velocity range of about 8 km s^{-1}. These observations recovered only about half the flux of the NRO observations and evidently revealed only the most prominent of the clouds in this complex. Vogel, Boulanger, and Ball found that the size and brightness of the CO cloud they detected was very nearly the same as that which would be observed from the Orion molecular cloud complex if it were at the same distance. These observations clearly support the contention that the CO features mapped by our NRO observations are indeed individual GMCs in M31, similar to those in our Galaxy.

It is interesting to consider our observations of M31 in the context of stellar and molecular cloud formation and evolution. From Figure 2 we see that the positions of the H II regions occur closer to the positions of peak CO emission rather than peak H I emission in the P248 and BA 292 cloud complexes, suggesting that, as in the Milky Way, the formation of massive stars occurs in molecular clouds. Figures 1 and 2 also show that the molecular coluds are well centered within the H I arm. As seen in Figure 1 and discussed earlier, the optically identified dark clouds, like the CO emission in D118, also appear centered along the spine of the H I arm. If the molecular gas is indeed centered within the H I filament, then this would suggest that the H I arm is itself centrally condensed along its length. Such an idea is consistent with the fact that the molecular complexes are regions of enhanced total mass density in the H I arm. This is what one might expect as a result of a gravitational (or Parker-type) instability in the H I arm. Spiral density waves appear capable of triggering such

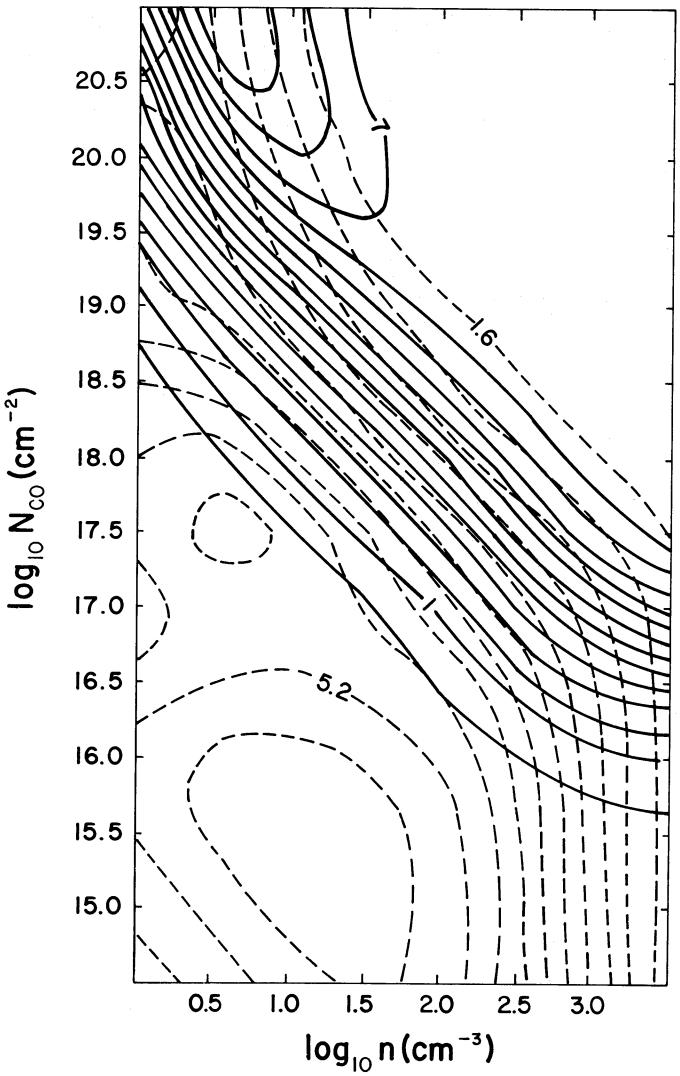

FIG. 12.—Predicted intensities of the $J = 1 \rightarrow 0$ transition of CO (*solid lines*) and the ratios of the $J = 1 \rightarrow 0$ to $J = 2 \rightarrow 1$ peak intensities (*dashed lines*) from a simple statistical equilibrium, radiative transfer calculation, representing a plane-parallel molecular cloud with a kinetic temperature of 10 K and a CO linewidth of 10 km s^{-1}. These quantities are plotted as a function of molecular hydrogen number density and CO column density. The solid contours are the peak temperatures of the $J = 1 \rightarrow 0$ transition expressed in equal 0.5 K units starting from 0.5 K at the lowest contour. The dashed contours run from 1.6 to 5.6 in equal increments of 0.4.

large-scale instabilities in disk galaxies (Elmegreen 1979). The very large arm-interarm contrast in CO emission in M31 (Stark 1985) suggests that the GMC–H I complexes we have observed are likely to have been formed within the spiral arm feature. There are at least two ways in which the GMCs could have been created within the H I arm. First, the deep potential well resulting from the large-scale instability in the arm could have collected into the H I arm numerous, preexisting, but undetectable, small interarm molecular clouds. Large, detectable GMCs would then form from these small molecular clouds through collisional coalescence. Second, the GMCs may have formed from atomic gas within the spiral arm feature. In this picture the interarm gas is primarily atomic hydrogen in form and the gravitational (or Parker) instability initially produces a central H I mass condensation which grows from the infall of surrounding gas until the column density of H I is above the threshold for molecular hydrogen then later CO formation. At this point the molecular complexes would become detectable. Our findings that (1) the overall molecular hydrogen mass in the arm is on the order of only 20% of the total gaseous mass, and (2) the H I and CO column densities are linearly correlated, combined with the fact that (3) the arm-interarm contrast in CO emission (≥ 25; Stark 1985) is considerably greater than that in H I emission (2–6; Sofue and Kato 1981) suggest that the molecular clouds were formed from the H I gas in the arm. Otherwise, (2) would imply that the arm-interarm contrast would be the same for CO and H I emission, which is inconsistent with (3). In other words, a population of small clouds with sufficient molecular mass to ultimately form the observed GMCs would be readily detectable in the interarm region. In addition, (1) indicates that the atomic gas is the largest reservoir of protons in the region and this is what one would expect if molecules formed from atomic gas in the H I arm. However, if the GMCs formed from atomic gas in the arm, (2) suggests that the conversion of H I $\rightarrow$ H_2 is never complete, even after the threshold column density for H_2 formation is exceeded. On scales of 100 parsecs or so the formation efficiency of H_2 from H I is between 50% and 70% (by mass). These considerations suggest that the molecular clouds we have observed are very young, having formed within a time given by $\tau_{GMC} \approx D_{H\,I} \div V_d \approx 2.0 \times 10^7$ yr, where $D_{H\,I}$ is the width of the H I arm above the column density threshold for CO detection (about 100 pc) and V_d is the velocity dispersion of the CO clouds in the arm (about 6 km s^{-1}). Finally, we point out that on scales of 100 pc or so we find no indication for a global spatial separation of the atomic and molecular gas as might be expected if a spiral density wave was responsible for the direct transformation of atomic to molecular gas in a shock. However, such a spatial segregation might not be apparent in M31 because of its high inclination to the line of sight. Consequently, our observations also could be consistent with molecular cloud formation in a classical density wave shock.

Apparently, soon after the formation of the GMCs takes place, OB star formation occurs within them. The formation of such stars is expected to eventually disrupt the GMCs. How long this takes is unclear. However, our observations of the A22 region suggest that this disruption process may also occur on a very short time scale. Figures 3 and 5 show our CO and H I observations centered on the H II region BA 289, a very bright nebula at the southwest tip of A22. The basic properties of the H I and CO emission here are considerably different from those found for the D118 region as a whole. For example, Figure 3 shows that the CO emission is weaker and more patchy in its spatial distribution than that of the D118 region. However, the most dramatic difference between the two regions is in the observed line widths of the H I and CO profiles. As Figure 5 and Table 1 show the H I emission toward BA 289 has a line width of about 53 km s^{-1}, nearly twice as wide as the typical H I profiles in the D118 region. The CO line toward BA 289 has a formal half-intensity width of 12 km s^{-1}, typical of the CO clouds near P248 and BA 292. However, unlike those clouds, significant CO emission from BA 289 is observed over a velocity range of nearly 40 km s^{-1} at just below the half-intensity level. It is important to note that the large velocity widths observed in the H I and CO gas are both localized and centered around BA 289. These large velocity dispersions are certainly associated with the H II region and

are not due to lots of small clouds which are distributed over a large distance along the line of sight in the highly inclined galaxy.

In Table 2 we list the atomic and molecular gas masses for the BA 289 region. Although the total gas mass associated with BA 289 is similar to that of the GMC complexes in D118 (i.e., $\sim 10^6\ M_\odot$), the fraction of the total mass along the entire line of sight in the form of molecular hydrogen is significantly lower, having a value of only about 30% or less. The viral mass for BA 289 is found to be about $10^7\ M_\odot$, an order of magnitude greater than the total mass listed in Table 2. Clearly, unlike the cloud complexes in D118, the BA 289 complex is unbound. The gravitational binding energy of an individual GMC in D118 is $\approx GM^2/R \approx 2 \times 10^{51}$ ergs which is approximately equal to the total kinetic energy of the gas in it. Toward BA 289 the kinetic energy (i.e., $\frac{1}{2}MV^2$) of the atomic hydrogen gas alone is roughly 7×10^{51} ergs and the total gas kinetic energy exceeds 10^{52} ergs! Apparently, massive stars in BA 289 and in A22 have injected large amounts of energy into the complex and through the combined action of H II regions, winds, and supernovae, have caused it to become unbound. Indeed, the overall morphology of the region (see Fig. 1) suggests that BA 289 is now located in the last surviving molecular remnant of a once larger molecular cloud complex from which the A22 association formed. The relative positions of the OB stars in A22, the H II region and the molecular gas are also consistent with a picture that the cloud disruption occurred as a result of the sequential progression of massive star formation through the original cloud (Elmegreen and Lada 1977). In any event, it appears that the time scale for cloud disruption by star formation is relatively short, since the BA 289 complex is not displaced in any measurable way from the spine of the H I arm. As before this suggests a time scale of disruption also on the order of a few times 10^7 yr.

Together, these considerations suggest that GMCs in this region of M31 are formed and destroyed over relatively short times within the H I spiral arm feature. This suggestion is consistent with the finding that the arm-interarm contrast in CO emission in M31 is very large (Stark 1985). These observations appear to indicate once more that spiral arms play a significant and fundamental role in the formation of GMCs and massive stars in disk galaxies, although, the detailed nature of that role is still unclear (e.g., Elmegreen 1987).

V. SUMMARY AND CONCLUSIONS

We have obtained the first coordinated CO and H I observations of M31 made with identical and sufficiently high angular and velocity resolutions to resolve individual giant molecular clouds. We obtained extensive observations of a star-forming complex located within a portion of a spiral arm about 7 kpc from the center of M31. The primary results of these observations can be summarized as follows.

1. The distribution of atomic and molecular gas is clearly correlated in both space and velocity. The peak temperatures and integrated intensities of H I and CO emission are found to be linearly related, with the strongest CO emission occurring in regions of strongest H I emission within the spiral arm.

2. The H I line widths are typically around 25 km s^{-1} and usually a factor of 2 broader than CO lines detected along the same lines of sight. Along lines of sight where both CO and H I lines are detected, the velocities of peak H I and CO emission tend to agree, but there is a large dispersion in the difference of peak emission velocities of about 6 km s^{-1}. However, in spite of this large dispersion, the extent of the CO emission is always contained within the extent of the H I emission profile. The dispersion in observed radial velocities of the CO clouds is between 4 and 6 km s^{-1} in the region observed. This is similar to the one-dimensional velocity dispersion of GMCs in the Milky Way.

3. The spatial distribution of CO emission toward D118 shows significant structure with a large contrast between the peaks of CO emission and the background, where no CO emission is detected. Indeed, the observations resolve the CO emission into three distinct cloud complexes with projected sizes and separations on the order of 100 pc. The distribution of H I emission is much smoother than that of the CO emission. However, spatial peaks in the H I intensity distribution are found at the same locations as the CO peaks. The contrast between the peaks and the background is considerably smaller for the H I emission than for the CO emission.

4. The molecular clouds are associated with H II regions and appear to be active sites of star formation. The clouds contain molecular hydrogen masses on the order of $5 \times 10^5\ M_\odot$, similar to the GMCs near the Sun. The GMCs in M31 are also found to contain substantial amounts of atomic hydrogen gas which comprise $\sim 30\%$ of the total mass of each cloud complex. These GMC–H I complexes are gravitationally bound and represent localized mass enhancements in the large H I spiral arm feature. The molecular component of each complex is made up of typically two or more large or intermediate-sized molecular clouds. There is no evidence for a significant contribution to the observed emission from small molecular clouds, indicating that masses of the complexes are dominated by GMCs.

5. The observed correlations between CO and H I intensities suggest a threshold column density for the formation of molecular hydrogen of about 10^{21} atomic hydrogen atoms per square centimeter. Similarly, the observations suggest a threshold atomic hydrogen density of about 5×10^{21} cm^{-2} for the formation of CO molecules. In both instances the apparent thresholds are very similar to the corresponding values observationally determined for clouds in the Milky Way. This suggests that the physical conditions (e.g., interstellar radiation field, gas-to-dust ratio, CO-to-H ratio, etc.) in the interstellar medium of M31 are similar to those in the solar neighboorhood.

6. In the region we mapped, about 25% of total gas mass is in the form of molecular hydrogen. For the spiral arm as a whole we estimate that 15%–20% of the total gaseous mass is in the form of molecular hydrogen. This is similar to the observed molecular hydrogen abundance within the solar neighborhood.

7. Comparison of CO observations in the $J = 1 \rightarrow 0$ and $J = 2 \rightarrow 1$ transitions with model cloud calculations suggest hydrogen number densities and CO column densities similar to those in galactic GMCs.

8. Comparison of our H I and CO observations suggests that molecular clouds form from atomic gas on relatively short time scales within a spiral arm. However, it is not clear whether this occurs as the result of a density wave shock or some sort of instability induced in the arm. Observations of large line widths associated with the atomic and molecular gas around the BA 289 H II region suggest that the formation of massive stars can lead to the rapid disruption of the molecular complexes after the clouds are formed. The entire evolution of the

GMCs in this region of M31 from formation to destruction may occur within a period of less than 10^8 yr.

Our observations indicate that the physical conditions in the D118 star-forming region of M31 are remarkably similar to those in the solar neighborhood of the Milky Way. The observed sizes, masses, atomic to molecular gas abundances, cloud densities, and velocity dispersions are all very similar to those of nearby GMCs. There is even some evidence to suggest that the gas-to-dust ratios and average interstellar radiation fields are similar. All of this is in striking contrast to a comparison of the global star-forming properties of the two galaxies. Although the two galaxies have similar total stellar and H I masses, M31 is 5 times weaker in its total far-infrared luminosity (Habing *et al.* 1984; Walterbos 1986) and has an average molecular hydrogen surface density between 3 and 5 times lower than the Milky Way (Walterbos [1986] and references therein). Our observations indicate that these global differences may not arise as a result of fundamental differences in the physical conditions of the interstellar medium on microscopic (i.e., 100 pc) scales. It is also clear that the star-formation properties of the Milky Way differ from M31 primarily in the inner regions of both galaxies. Perhaps the pertinent question which needs to be addressed is why the inner Milky Way is so different from the solar neighborhood in its star-formation properties.

We gratefully acknowledge useful discussions with John Black, Leo Blitz, Bruce Elmegreen, Tetsuo Hasegawa, Philip Jewell, Walter Kailey, Philip Maloney, and Stuart Vogel. We thank Arnold Rots and J. van Gorkom for assistance with the VLA data reduction. We are grateful to Takashi Iosbe and Eric Feigelson for deriving for us the statistical correlations describing our data when both upper limits and actual detections are incorporated. We particularly thank Stuart Vogel for pointing out an error in an early version of this manuscript and for providing data in advance of publication. This research was supported in part by NSF grant AST 82-10463 and by the Arizona Submillimeter Telescope Project. Y. S. thanks the Ministry of Education of Japan for financial support under grant no. 61460009.

REFERENCES

Baade, W., and Arp, H. 1964, *Ap. J.*, **139**, 1027.
Blitz, L. 1985, *Ap. J.*, **296**, 481.
———. 1987, preprint.
Blitz, L., and Thaddeus P. 1980, *Ap. J.*, **241**, 676.
Bloemen, J. B. G. M., *et al.* 1986, *Astr. Ap.*, **154**, 25.
Boulanger, F., Stark, A. A., and Combes F. 1981, *Astr. Ap.*, **93**, L1.
Boulanger, F., Bystedt, J., Casoli, F., and Combes, F. 1984, *Astr. Ap.*, **140**, L5.
Brinks, E. 1984, unpublished Ph.D. dissertation, Leiden.
Combes, F., Encrenaz, P. J., Lucas, R., and Weliachew, L. 1977, *Astr. Ap.*, **225**, 346.
Elmegreen, B. G. 1987, in *IAU Symposium 115: Star Forming Regions*, ed. M. Piembert and J. Jugaku (Dordrecht: Reidel), p. 457.
Elmegreen, B. G. 1979, *Ap. J.*, **231**, 372.
Elmegreen, B. G., and Elmegreen, D. M. 1987, *Ap. J.*, **314**, 3.
Elmegreen, B. G., and Lada, C. J. 1977, *Ap. J.*, **214**, 725.
Emerson, D. J. 1976, *M.N.R.A.S.*, **176**, 321.
Feigelson, E. D., and Nelson, P. I. 1985, *Ap. J.*, **293**, 192.
Gordon, C. P. 1970, *A.J.*, **75**, 914.
Habing, H. J., *et al.* 1984, *Ap. J.* (*Letters*), **278**, 59.
Hasegawa, T., Sato, F., and Fukui, Y. 1983, *A.J.*, **88**, 658.
Hodge, P. W. 1981, *Atlas of the Andromeda Galaxy* (Seattle: University of Washington Press).
Ichikawa, T., Nakano, M., Tanaka, Y. D., Saito, M., Nakai, N., Sofue, Y., and Kaifu, N. 1985, *Pub. Astr. Soc. Japan*, **37**, 439.
Isobe, T., Feigelson, E. D., and Nelson, P. I. 1986, *Ap. J.*, **306**, 490.
Kutner, M. L., Mundy, L., and Howard, R. J. 1984, *Ap. J.*, **283**, 890.
Kutner, M. L., and Ulich, B. L. 1981, *Ap. J.*, **250**, 341.
Lada, C. J., Elmegreen, B. G., Cong, H-I., and Thaddeus, P. 1978, *Ap. J.* (*Letters*), **226**, 39.
Lada, E. A., and Blitz, L. 1987, preprint.
Linke, R. 1981, in *Extragalactic Molecules*, ed. L. Blitz and M. L. Kutner (Green Bank: NRAO Publ.), p. 87.
Maddalena, R. J., Morris, M., Moscowitz, J., and Thaddeus P. 1986, *Ap. J.*, **303**, 375.
Magnani, L., Lada, E. A., and Blitz, L. 1986, *Ap. J.*, **301**, 395.
Margulis, M., and Lada, C. J. 1985, *Ap. J.*, **299**, 925.
———. 1986, *Ap. J.* (*Letters*), **309**, 87.
Nakano, M., Ichikawa, Y. D., Tanaka, N., Nakai, N., and Sofue, Y. 1987, *Pub. Astr. Soc. Japan*, in press.
Pellet, A., Astier, N., Viale, A., Courtes, G., Monnet, G., and Simien, F. 1978, *Astr. Ap. Suppl.*, **31**, 439.
Sandage, A., and Tammann G. 1968, *Ap. J.*, **151**, 525.
Sanders, D. B., Solomon, P. M., and Scoville, N. Z. 1984, *Ap. J.*, **276**, 182.
Savage, B. D., and Mathis, J. S. 1979, *Ann. Rev. Astr. Ap.*, **17**, 73.
Savage, B. D., Bohlin, R. C., Drake, J. F., and Budich, W. 1977, *Ap. J.*, **216**, 291.
Sofue, Y., and Kato, T. 1981, *Pub. Astr. Soc. Japan*, **33**, 449.
Spitzer, L. 1978, in *Physical Processes in the Interstellar Medium* (New York: Wiley), p. 43.
Stark, A. A. 1985, in *IAU Symposium 106: The Milky Way Galaxy*, ed. H van Woerden, R. J. Allen, and B. Burton (Dordrecht: Reidel), p. 445.
Ulich, B. L., and Haas, R. W. 1976, *Ap. J. Suppl.*, **30**, 427.
Unwin, S. C. 1980, *Astr. Ap. Suppl.*, **55**, 179.
van Dishoeck, E. F., and Black, J. H. 1987, preprint.
Vogel, S., Boulanger, F., and Ball, R. 1987, *Ap. J.* (*Letters*), **321**, L145.
Walterbos, R. 1986, unpublished Ph.D. dissertation, Leiden.
Wannier, P. G., Lichten, S., and Morris, M. 1983, *Ap. J.*, **268**, 727.

CHARLES J. LADA and MICHAEL MARGULIS: Steward Observatory, University of Arizona, Tucson, AZ 85721

TOSHIHIRO HANDA, NAOMASA NAKAI, and YOSHIAKI SOFUE: Nobeyama Radio Observatory, Tokyo Astronomical Observatory, University of Tokyo, Nobeyama, Minamisaku, Nagano 384-13, Japan